nature research
https://doi.org/10.1038/s41586-020-3030-1

Supplementary information

Plasmonic topological quasiparticle on the nanometre and femtosecond scales

In the format provided by the authors and unedited

Supplemental Information

Here, we present an analytical model of a plasmonic vortex, and based on analysis of the designed topological charge, identify the generated quasiparticles as merons. We formulate an analytical theory for determining the SPP fields and their spin textures produced by illuminating the Archimedean coupling structure with linearly polarized light. The model explains how the designed plasmonic OAM creates one primary and two secondary plasmonic vortices, which support topological spin textures with a total 3/2 meron-like nontrivial topological charge.

A. Analytical formalism of the Plasmonic Vortex Fields.

Our analysis and assignment of the quasiparticle topological SAM texture in the main text is based on ITR-PEEM imaging of plasmonic vortices and their FDTD simulations. We present a complementary analytical model that confirms the assignment to a meron type SAM texture and provides an intuitive basis for design of plasmonic topological spin textures grounded on how the geometric charge tailors the nanometer spatial and femtosecond temporal SPP fields that are implicit in their formulation in terms of Bessel functions.

We consider an array of point sources of SPP waves distributed with the Archimedean coupling structure geometry at a metal/dielectric interface; each point is a source of $\mathbf{E}_{\mathrm{z}}$ and $\mathbf{E}_{\mathrm{long}}$ electric fields (see Extended Data Fig. 1), as well as a magnetic component $\mathbf{H}_{\parallel}$ parallel to the surface and orthogonal to both $\mathbf{E}_{\mathrm{z}}$ and $\mathbf{E}_{\mathrm{long}}$. The launching from each point source and propagation of SPP fields at the vacuum/Ag interface is described in cylindrical coordinates as follows,[1]

$$\mathbf{E}_{\mathrm{z}} = -\frac{k_{\mathrm{SPP}}}{\omega_{\mathrm{SPP}}\varepsilon_0\varepsilon_{\mathrm{d}}} e^{i(\mathbf{k}_{\mathrm{SPP}}\cdot\mathbf{r}-\omega_{\mathrm{SPP}}t)} e^{-\kappa z}\mathbf{e}_{\mathrm{z}}, \tag{$S1.1$}$$

$$\mathbf{E}_{\mathrm{long}} = i\frac{\kappa}{\omega_{\mathrm{SPP}}\varepsilon_0\varepsilon_{\mathrm{d}}} e^{i(\mathbf{k}_{\mathrm{SPP}}\cdot\mathbf{r}-\omega_{\mathrm{SPP}}t)} e^{-\kappa z}\mathbf{e}_{\mathrm{r}}, \tag{$S1.2$}$$

$$\mathbf{H}_{\parallel} = e^{i(\mathbf{k}_{\mathrm{SPP}}\cdot\mathbf{r}-\omega_{\mathrm{SPP}}t)}e^{-\kappa z}\mathbf{e}_{\varphi}, \tag{S1.3}$$

where $i = \sqrt{-1}$, $\mathbf{e}_{\mathrm{r}(\varphi,\mathrm{z})}$ are unit vectors in the radial (azimuthal, and transverse) directions with respect to a point source on the Archimedean coupling structure, κ is its imaginary wave vector normal to the surface, $\varepsilon_0\varepsilon_{\mathrm{d}}$, the dielectric constant (for vacuum $\varepsilon_{\mathrm{d}} = 1$), and $e^{i(\mathbf{k}_{\mathrm{SPP}}\cdot\mathbf{r}-\omega_{\mathrm{SPP}}t)}$, the SPP phase evolving with spatial and temporal frequencies $\mathbf{k}_{\mathrm{SPP}}$ and ω_{SPP} over a distance $|\mathbf{r}|$ and time t. The term $e^{-\kappa z}$ is dropped because photoemission measures the field strength at the interface (z=0), and $e^{i\omega_{\mathrm{SPP}}t}$ is first treated as a constant to obtain time independent solutions.

With SPP fields described by these standard forms emanating from point sources on the Archimedean spiral coupling structure, we propagate them to calculate how the OAM forms a vortex, and through spin-orbit interaction of light, the resulting SAM texture.[2-6] To minimize the mathematical complexity, the source is modeled as a single-opening spiral (Fig. S1a) carrying the equivalent geometric charge as the experimental multiple-element one; the equivalency of geometrical charges has been established, though one expects minor differences in the generated SPP fields to arise from diffraction at the structure edges.[7] The coupling structure in Fig. S1a is described in cylindrical coordinates $(r, \varphi, z = 0)$, where the change in its radius r with the azimuthal angle φ defines its geometric charge m, and therefore, the OAM of the generated SPP field. The propagated SPP fields are evaluated at points $(R, \Theta, \mathrm{z} = 0)$, sharing the same origin (x, y=0) as the source field. To examine how the OAM evolves into the SAM texture, we derive the SPP field at point $(R, \Theta, 0)$ near the vortex by propagating and integrating the vectorial fields from each point source, $\mathbf{E}_{\mathrm{PS}}(r, \varphi, 0)$.[8] In Eqs. (S2), the total $\mathbf{E}_{\mathrm{z}}$-component is expressed as,

$$\mathbf{E}_{\mathrm{z}}(R, \Theta, 0) = \int \mathbf{E}_{\mathrm{z,PS}}(R, \Theta, 0)\, r d\varphi \tag{S2.1}$$

$$= \mathbf{e}_z \int -\frac{k_{\mathrm{SPP}}}{\omega_{\mathrm{SPP}}\varepsilon_0\varepsilon_{\mathrm{d}}} e^{i\mathbf{k}_{\mathrm{SPP}}\cdot\mathbf{L}} r\cos\varphi d\varphi \quad \text{(S2.2)}$$

$$= \mathbf{e}_z \int -\frac{k_{\mathrm{SPP}}}{\omega_{\mathrm{SPP}}\varepsilon_0\varepsilon_{\mathrm{d}}} e^{-ik_{\mathrm{SPP}}\mathbf{e}_{\mathrm{r}}\cdot\left[R\mathbf{e}_{\mathrm{R}}-\left(r_0+\frac{m\lambda_{\mathrm{SPP}}}{2\pi}\varphi\right)\mathbf{e}_{\mathrm{r}}\right]} \left(r_0 + \frac{m\lambda_{spp}}{2\pi}\varphi\right)\cos\varphi d\varphi \quad \text{(S2.3)}$$

$$\cong \mathbf{e}_z \frac{-r_0 k_{\mathrm{SPP}}}{\omega_{\mathrm{SPP}}\varepsilon_0\varepsilon_{\mathrm{d}}} \int e^{-ik_{\mathrm{SPP}}R\mathbf{e}_{\mathrm{r}}\cdot\mathbf{e}_{\mathrm{R}}} e^{ik_{\mathrm{SPP}}r_0} e^{im\varphi} \frac{e^{i\varphi}+e^{-i\varphi}}{2} d\varphi \quad \text{(S2.4)}$$

$$= \mathbf{e}_z \frac{-\pi r_0 k_{\mathrm{SPP}}}{\omega_{\mathrm{SPP}}\varepsilon_0\varepsilon_{\mathrm{d}}} e^{ik_{\mathrm{SPP}}r_0} i^{-(m+1)} e^{i(m+1)\Theta}\left[J_{m+1} - e^{-2i\Theta}J_{m-1}\right]. \quad \text{(S2.5)}$$

To evaluate the fields at $(R,\Theta,0)$, the contribution from each point source at $(r,\varphi,0)$ is propagated by $\mathbf{L} = R\mathbf{e}_{\mathrm{R}} - \left(r_0 + \frac{m\lambda_{\mathrm{SPP}}}{2\pi}\varphi\right)\mathbf{e}_{\mathrm{r}}$, where $\mathbf{e}_{\mathrm{R}}$ is the radial unit vector in the vortex coordinate frame (Fig. S1a). Considering that for the experimental $r_0 = 19\lambda_{\mathrm{SPP}} \gg \lambda_{\mathrm{SPP}} \sim R$ holds, we make two approximations: 1) The radius variation term, $r_0 + \frac{m\lambda_{\mathrm{SPP}}}{2\pi}\varphi$ in the last parenthesis of Eq. (S2.3) is dropped; 2) The SPP $\mathbf{k}$-vector is approximated as $\mathbf{k}_{\mathrm{SPP}} = k_{\mathrm{SPP}}\frac{\mathbf{L}}{|\mathbf{L}|} \approx -k_{\mathrm{SPP}}\mathbf{e}_{\mathrm{r}}$, because $|\mathbf{L}| \gg R$. Note that the $r_0 + \frac{m\lambda_{\mathrm{SPP}}}{2\pi}\varphi$ term must be retained in the exponential that accounts for the SPP propagation, because its φ dependence determines the geometric charge and, ultimately, its effect on spin-orbit coupling. The spin-orbit coupling is embodied in order of the Bessel integral n, involving functions of the first kind, $J_n = J_n(\mathrm{Re}(k_{\mathrm{SPP}})R)$, where we use the real part of $\mathbf{k}_{\mathrm{SPP}}$ because it is $\sim 10^3$ greater than its imaginary part in the visible spectrum.[1] The $\cos\varphi$ term in Eq. (S2.2) accounts for the angular coupling efficiency of linearly polarized light at various points of the structure, which is expressed in Eq. (S2.4) as $\frac{e^{i\varphi}+e^{-i\varphi}}{2}$ to facilitate the integration.[9] Only the parallel, not the orthogonal, component of the optical field to $\mathbf{k}_{\mathrm{SPP}}$ can launch the SPP fields.[10]

We note from Eq. (S2.5) that $\mathbf{E}_z$ is a superposition of two Bessel functions of different orders (J_{m-1}, J_{m+1}), which are defined by the geometric charge of the spiral coupling structure, and thus are labeled by the index m. Considering that linearly polarized light can be represented as a superposition of the left and right circularly polarized components (LCP and RCP) carrying SAM quantum number of σ=±1 [Eq. (S2.4)], the total SPP field is also as a superposition of two component fields with OAM of m-1 and m+1 accounting for J_{m-1} and J_{m+1}, respectively.[8] The two component fields form own vortices defined by their OAM, which when superposed define the total SPP fields and their topological plasmon spin texture, as will be shown. Similarly, by integrating the propagated $\mathbf{E}_{\mathrm{long}}$ and $\mathbf{H}_{\parallel}$, we express the SPP electric and magnetic fields at (R,Θ,0), accordingly:

$$\mathbf{E}_{\mathrm{R}}(R,\Theta,0)=\mathbf{e}_{\mathrm{R}}\frac{\pi i\kappa r_0}{2\omega_{\mathrm{SPP}}\varepsilon_0\varepsilon_{\mathrm{d}}}e^{ik_{\mathrm{SPP}}r_0}i^m e^{i(m+1)\Theta}\left[(J_m-J_{m+2})+e^{-2i\Theta}(J_m-J_{m-2})\right],\qquad (S3.1)$$

$$\mathbf{E}_{\Theta}(R,\Theta,0)=\mathbf{e}_{\Theta}\frac{-\pi\kappa r_0}{2\omega_{\mathrm{SPP}}\varepsilon_0\varepsilon_{\mathrm{d}}}e^{ik_{\mathrm{SPP}}r_0}i^m e^{i(m+1)\Theta}\left[e^{-2i\Theta}(J_m+J_{m-2})-(J_m+J_{m+2})\right],(S3.2)$$

$$\mathbf{H}_{\mathrm{R}}(R,\Theta,0)=\mathbf{e}_{\mathrm{R}}\frac{\pi r_0}{2i}e^{ik_{\mathrm{SPP}}r_0}i^m e^{i(m+1)\Theta}\left[e^{-2i\Theta}(J_m+J_{m-2})-(J_m+J_{m+2})\right],\ (S3.3)$$

$$\mathbf{H}_{\Theta}(R,\Theta,0)=\mathbf{e}_{\Theta}\frac{\pi r_0}{2}e^{ik_{\mathrm{SPP}}r_0}i^m e^{i(m+1)\Theta}\left[(J_m-J_{m+2})+e^{-2i\Theta}(J_m-J_{m-2})\right],\ (S3.4)$$

$$\mathbf{H}_{\mathrm{z}}(R,\Theta,0)=0,\qquad (S3.5)$$

where it is again evident that the in-plane fields can also be decomposed into two vortices of OAM of m-1 and m+1, defined by $(J_m \pm J_{m-2})$ and $(J_m \pm J_{m+2})$, respectively. A comparison of absolute values of the electric field components (normalized with respect to the incident field) in cylindrical coordinates between the FDTD and analytical models is plotted in Fig. S1b for m=2, where a nearly exact correspondence is evident, and justifies further analytical modeling based on the simplified source structure and other mathematical approximations. The time dependence of the vortex fields can be restored by multiplying the SPP field expressions in Eq. (S2) and (S3) by $e^{-i\omega_{\mathrm{SPP}}t}$ and converting into Cartesian coordinates, as shown in Extended Data Fig. 5.

To illustrate how the vortex fields generate meron spin textures, in Fig. S2a,b, we separately present the $\mathbf{E}_z$ fields of vortices that are generated by the LCP and RCP components of the linearly polarized optical field as they evolve in 100 as time steps within a 400 as time window. In addition, since the two components act together, Fig. S2c displays their sum, the total SPP $\mathbf{E}_z$ field, overlaid with the calculated L-line map evaluated from $1/|P_3|$. We choose to report the $\mathbf{E}_z$ fields because 1) they have suggestive phase structure centered on the phase singularity at the vortex core, which makes them conceptually straightforward to visualize orbiting vortices with a defined OAM (i.e. m-1 and m+1), and 2) it is convenient to identify the quasiparticle north/south poles, which are generated by circulation of the pure in-plane fields around the phase singularities in the total $\mathbf{E}_z$ field, as will be discussed later. Note that similar analysis can be done with the radial and tangential components, but not the *x*- and *y*-components of $\mathbf{E}_{\text{long}}$ because the former also possess the rotational symmetry. The total fields define the physics, but it is easier to conceptualize it by considering just the $\mathbf{E}_z$ component.

In the following discussions, we refer to the two vortices with OAM of m-1 and m+1 as the generating-vortices. In the case of m=2, Their $\mathbf{E}_z$ fields have radial and azimuthal interferences that circulate about the vortex core, where their amplitudes are zero. Note, the properties of Bessel functions are such that as long as $m \neq 0$ increases, the first radial destructive interference for each vortex (dotted circle in Fig. S2a,b) moves out to a larger r from the core, while the second and subsequent ones are nearly independent of m as r is increased, and oscillate in radial direction with a period of $\approx \lambda_{\text{SPP}}$; this crucially defines the spatial overlap of the generating-vortices where spin-orbit interaction is strongest, and thus the consequent SPP spin texture.

Next, we consider how superposition of the two generating vortices affects the SPP fields and SAM away from their phase singularities. First, the superposition maintains the common central phase singularity of the two generating-vortices, and locates the central hourglass L-line domain; its dimension is defined by the OAM=1 generating-vortex because it varies faster with r compared with OAM=3. Second, the OAM (1 and 3) of the generating-vortices defines their circulation angular frequencies of $2\pi/1$ and $2\pi/3$ per optical cycle, as can be visualized by the rotation of phase fronts of the azimuthal destructive interferences, as well as constructive interferences (the vortex petals; marked by rotating black dotted and dashed lines in Fig. S2a,b, respectively). Because of their different circulation rates, the two generating vortices spatially bifurcate when going from in-phase to out-of-phase, and adjoin once they return to in-phase; this cycling from in- and out-of-phase thus generates an infinite number of C-point phase singularities. At center of the excitation pulse, these additional phase singularities will be aligned exactly along the y and x axis. Of all these side phase singularities, however, only the central vortex and the first two side ones along the y axis (black dots in Fig. S2c) contribute to a nonzero system topological charge, because they are not paired with corresponding oppositely circulating phase singularities along the x axis, as will be shown. The field circulation of these two side phase singularities is marked by the arrows in Fig. S2c, which is partially reflected in the y-component of $\mathbf{E}_{\text{long}}$ (Extended Data Fig. 5, middle row), and is also captured experimentally in the SI Video 2. Therefore, these first two side phase singularities that are displaced by $\pm y \approx 1/2\lambda_{\text{SPP}}$ from y=0 are special; recognizing their circulating total fields we refer to them as the side-vortices to differentiate them from the generating vortices. Because of the different radius of the first 1/2 cycle of the Bessel functions of the generating-vortices, their strongest spatial overlap defines their $\pm y$ displacement at the center of the two side elliptical L-lines, as marked by black dots in Fig. S2c. Thus, we conclude that in the central region of the coupling structure, the interference of the two generating vortices with m dependent rotation speeds generates the total field, which can be interpreted as consisting of a primary vortex at the spiral center, and two effective side-vortices bounded by the two elliptical L-line lobes on each side of the central hourglass. As we show next, the significance of each of these domains is their associated SAM textures with topological charges of 1/2, corresponding to an SPP spin texture of a meron-like quasiparticle in Fig. 1, adding up to a total charge of 3/2 for the entire system.

B. Formalism of the Topological SAM Textures.

Having described the SPP fields that are created by illuminating an m=2 Archimedean structure with linearly polarized light, we calculate their SAM textures, according to Eqs. 1, (S2.5) and (S3.1-3.5). The SAM vectorial components can be expressed as,

$$\mathbf{S}_{\mathrm{R}}(R,\Theta,0)=\mathbf{e}_{\mathrm{R}}\varepsilon_{\mathrm{d}}\kappa k_{\mathrm{SPP}}\left(\frac{\pi r_0}{\omega\varepsilon_0\varepsilon_{\mathrm{d}}}\right)^2\begin{bmatrix}(\cos2\Theta-1)J_mJ_{m+1}-J_{m+1}J_{m+2}+\cos2\Theta J_{m-2}J_{m+1}+\\(\cos2\Theta-1)J_{m-1}J_m+\cos2\Theta J_{m-1}J_{m+2}-J_{m-2}J_{m-1}\end{bmatrix},(S4.1)$$

$$\mathbf{S}_{\Theta}(R,\Theta,0)=\mathbf{e}_{\Theta}\varepsilon_{\mathrm{d}}\kappa k_{\mathrm{SPP}}\left(\frac{\pi r_0}{\omega\varepsilon_0\varepsilon_{\mathrm{d}}}\right)^2\sin2\Theta[J_mJ_{m+1}-J_{m-2}J_{m+1}+J_{m-1}J_m-J_{m+2}J_{m-1}],(S4.2)$$

$$\mathbf{S}_{\mathrm{z}}(R,\Theta,0)=\mathbf{e}_{\mathrm{z}}\left[\frac{\varepsilon_{\mathrm{d}}}{2}\left(\frac{\pi\kappa r_0}{\omega\varepsilon_0\varepsilon_{\mathrm{d}}}\right)^2+\mu\left(\frac{\pi r_0}{2}\right)^2\right]\left[J_{m-2}{}^2-J_{m+2}{}^2-2cos2\Theta(J_{m-2}J_m-J_mJ_{m+2})\right].(S4.3)$$

The spin textures are defined by 1) the spin carried by the LCP and RCP optical fields, and, 2) the spin-orbit-interaction introduced by the coupling structure with a geometric charge $m=2$. The derived spin distribution is plotted in Fig. S3b, where the colormap shows the normalized $\mathbf{S}_{\mathrm{z}}$ component and the arrows indicate the normalized in-plane spin projections. We note that the spin vectors follow the field envelope of the generating light, because the time-dependent field oscillation terms cancel by multiplication with complex conjugates, according to Eq. 1. The spin distribution from the analytical model matches that of the FDTD simulation (Fig. 4b), and thus again validates both approaches. From the analytical spin distribution, we calculate the particle density, as defined by Eq. 2, to obtain the distribution in Fig. S3c. The density distribution is overlaid by the L-line map calculated from $1/|P_3|$ [Eq. (3.3)], to emphasize the excellent agreement with the FDTD plot in Fig. 4c. Integrating the particle density within the central hourglass L-line domain, we obtain a topological charge of Q=1/2, corresponding to a meron-like particle. Meron is a topological quasiparticle characterized by a spin texture that points vertically at the center and realigns by π/2 to an inward or outward horizontal orientation at its edge. Therefore the $\mathbf{S}_\mathrm{z} = 0$ condition with the same hourglass shape defines the central meron boundary (Fig. S3a), just as for the L-line maps from the FDTD and analytical calculations (Figs. 4a and S3a).

Although the FDTD and the analytical approaches describe the same quasiparticle, the latter provides better insights into the role of the geometrical charge of the coupling structure in conversion of the plasmon OAM into the SAM texture, i.e. the spin-orbit coupling (SOC). This can be illustrated by expressing Eq. (S4.3) as,

$$\mathbf{S}_\mathrm{z} = \mathbf{e_z}\left[\frac{\varepsilon_\mathrm{d}}{2}\left(\frac{\pi\kappa r_0}{\omega\varepsilon_0\varepsilon_\mathrm{d}}\right)^2 + \mu\left(\frac{\pi r_0}{2}\right)^2\right]\left[(J_m^2 - J_{m-2}^2) - (J_m^2 - J_{m+2}^2) + 2cos2\theta(J_mJ_{m-2} - J_mJ_{m+2})\right]. \quad (S5)$$

In this form, the first Bessel equation term $(J_m^2 - J_{m-2}^2)$ and the second term $(J_m^2 - J_{m+2}^2)$ describe the spin textures produced by the generating-vortices with OAM of *m*-1 and *m*+1, respectively, while the last term $(J_mJ_{m-2} - J_mJ_{m+2})$ conveys the interaction between the two generating-vortices due to the cross product in Eq. 1. This is the SOC term that converts the joint OAM of the SPP wave into its spin texture; it is diametric to a coupling structure with a geometric charge of *m* converting spin σ of circularly polarized light into an SPP wave with OAM of *m*+*σ*.[2,11] Together, these three Bessel function terms convey the conversion of OAM into the spin texture. Based on the above analysis, we can engineer different spin textures by predefining the plasmon fields and their interactions with structures having different geometric charges; for example, *m*=0 coupling structure excited by circularly polarized light produces a skyrmion spin texture, as we will report in a future publication.[12]

References:

1 Maier, S. A. *Plasmonics: fundamentals and applications*. (Springer Science & Business Media, 2007).

2 Bliokh, K. Y., Rodríguez-Fortuño, F. J., Nori, F. & Zayats, A. V. Spin–orbit interactions of light. *Nat. Photon.* **9**, 796-808 (2015).

3 Bliokh, K. Y., Smirnova, D. & Nori, F. Quantum spin Hall effect of light. *Science* **348**, 1448-1451 (2015).

4 Cardano, F. & Marrucci, L. Spin–orbit photonics. *Nat. Photon.* **9**, 776-778 (2015).

5 Kort-Kamp, W. J. d. M. Topological phase transitions in the photonic spin Hall effect. *Phys. Rev. Lett.* **119**, 147401 (2017).

6 Ling, X. *et al.* Recent advances in the spin Hall effect of light. *Rep. Prog. Phys.* **80**, 066401 (2017).

7 Kim, H. *et al.* Synthesis and Dynamic Switching of Surface Plasmon Vortices with Plasmonic Vortex Lens. *Nano Lett.* **10**, 529-536 (2010).
8 Yang, S., Chen, W., Nelson, R. L. & Zhan, Q. Miniature circular polarization analyzer with spiral plasmonic lens. *Opt. Lett.* **34**, 3047-3049 (2009).
9 Lin, J. *et al.* Polarization-controlled tunable directional coupling of surface plasmon polaritons. *Science* **340**, 331-334 (2013).
10 Dai, Y., Dąbrowski, M., Apkarian, V. A. & Petek, H. Ultrafast microscopy of spin-momentum-locked surface plasmon polaritons. *ACS Nano* **12**, 6588-6596 (2018).
11 Spektor, G. *et al.* Revealing the subfemtosecond dynamics of orbital angular momentum in nanoplasmonic vortices. *Science* **355**, 1187-1191 (2017).
12 Dai, Y. *et al.* Ultrafast Microscopy of a Plasmonic Spin Skyrmion. *arXiv preprint arXiv:1912.03826* (2019).

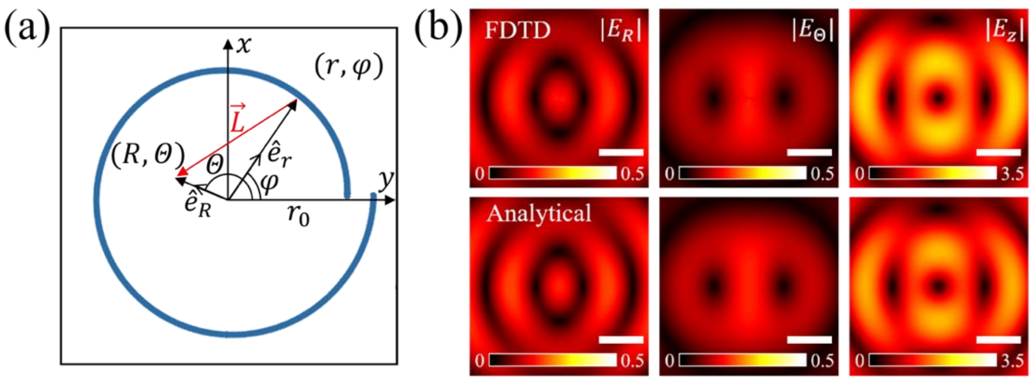

Figure S1 | The analytical model of the Archimedean coupling structure and comparison of its calculated SPP fields from with those from the FDTD calculation. **a,** Geometry and coordinates of the Archimedean spiral vortex coupling structure used for deriving the analytical model. **b,** Comparison between the moduli of the calculated normalized electric fields at the plasmonic vortex averaged over one optical cycle from the FDTD and analytical models, for m=2. The image size is $1 \times 1\ \mu m^2$. The scale bars indicate λ_{SPP}

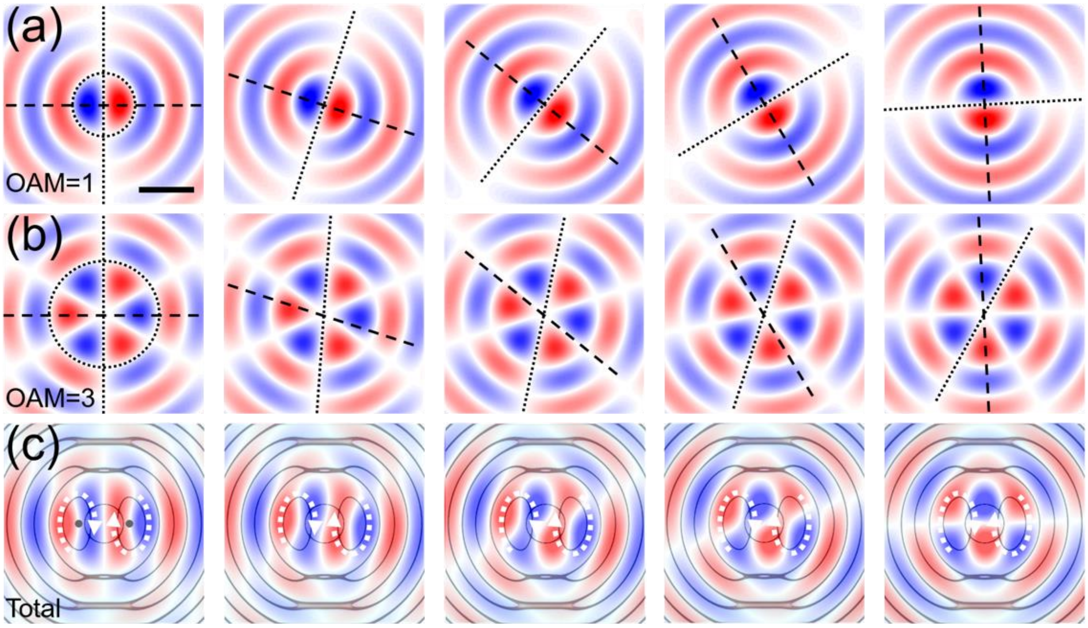

Figure S2 | The decomposition of the plasmon $\mathbf{E}_z$ fields into component vortices of SPPs with a, OAM=1 and **b**, OAM=3, respectively, evolving from left to right in 100 as time steps. The black dotted and dashed lines mark, respectively, the azimuthal destructive and constructive phase fronts of the generating vortices. The dotted circles mark the first radial destructive interference. The area shown is $2 \times 2\ \mu m^2$, with a scale bar indicating λ_{SPP} in (a). **c,** The total $\mathbf{E}_z$ field combining OAM=1 and 3 components, overlaid with the L-line map (dark contrast). The dashed arrows accentuate the circulation of the side lobes around the side phase singularities (gray dots).

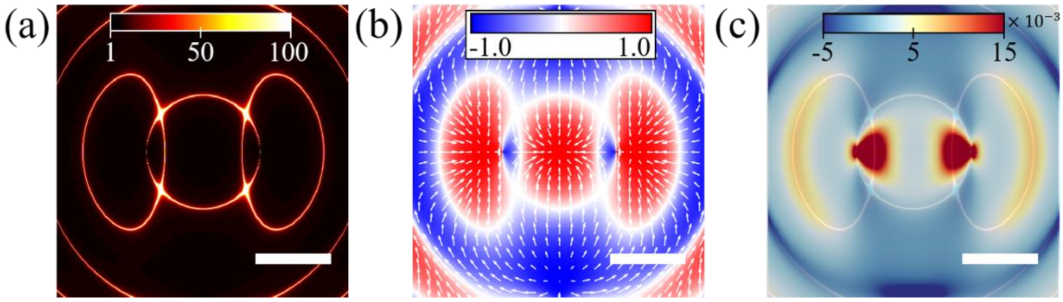

Figure S3 | The meron boundary and particle density from the analytical model. **a,** Colormap of the calculated inverse of the $|P_3|$ Stokes parameter, equivalent to the L-line map in Fig. 4a. The color scale amplitude ranges from 1 to infinity, respectively, correspond to the circular and linear polarization limits. **b,** The SAM texture at the vortex core. The colormap shows distribution of the normalized out-of-plane spin components, with arrows indicating the in-plane spin orientations. The white contrast showing $\mathbf{S}_z$=0 reproduces the L-line map in **a** and **c.** Colormap showing the particle density with the L-line distribution (white contrast) superposed. The obtained spin textures and L-lines from the analytical model are in excellent agreement with the results from numerical simulations shown in Fig. 4a-c in the main text.